Vol. 652: 15–32, 2020
https://doi.org/10.3354/meps13479

MARINE ECOLOGY PROGRESS SERIES
Mar Ecol Prog Ser

Published October 15

Food-web fluxes support high rates of mesozooplankton respiration and production in the equatorial Pacific

Michael R. Landry[1,*], Michael R. Stukel[2], Moira Décima[3,4]

[1]Scripps Institution of Oceanography, University of California, San Diego, 9500 Gilman Dr., La Jolla, California 92093-0227, USA

[2]Department of Earth Ocean and Atmospheric Sciences, Florida State University, Tallahassee, Florida 32303, USA

[3]National Institute of Water and Atmospheric Research, Hataitai, Wellington 6022, New Zealand

[4]*Present address:* Scripps Institution of Oceanography, University of California, San Diego, 9500 Gilman Dr., La Jolla, California 92093-0227, USA

ABSTRACT: We investigated how the network of food-web flows in open-ocean systems might support high rates of mesozooplankton respiration and production by comparing predicted rates from empirical relationships to independently determined solutions from an inverse model based on tightly constrained field-measured rates for the equatorial Pacific. Model results were consistent with estimates of gross:net primary production (GPP:NPP), bacterial production:NPP, sinking particulate export, and total export for the equatorial Pacific, as well as general literature values for growth efficiencies of bacteria, protozooplankton, and metazooplankton. Mean rate estimates from the model compared favorably with the respiration predictions from Ikeda (1985; *Mar Biol 85:1–11*) (146 vs. 144 mg C m^{-2} d^{-1}, respectively) and with production estimates from the growth rate equation of Hirst & Sheader (1997; *Mar Ecol Prog Ser 154:155–165*) (153 vs. 144 mg C m^{-2} d^{-1}). Metazooplankton nutritional requirements are met with a mixed diet of protozooplankton (39%), phytoplankton (36%), detritus (15%), and carnivory (10%). Within the food-web network, NPP of 896 mg C m^{-2} d^{-1} supports a total heterotrophic carbon demand from bacteria, protozoa, and metazooplankton that is 2.5 times higher. Scaling our results to primary production and zooplankton biomass at Stn ALOHA suggests that zooplankton nutritional requirements for high growth might similarly be met in oligotrophic subtropical waters through a less efficient trophic structure. Metazooplankton production available to higher-level consumers is a significant contributor to the total export needed for an overall biogeochemical balance of the region and to export requirements to meet carbon demand in the mesopelagic depth range.

KEY WORDS: Inverse analysis · Trophic fluxes · Feeding · Respiration · Growth rate · Production · Export · Mesopelagic carbon demand

1. INTRODUCTION

Despite the broadly recognized importance of zooplankton for secondary production, nutrient cycling, export, and trophic transfer in marine food webs (Steinberg & Landry 2017), the process rates underlying these functions are not easily or routinely measured in natural open-ocean communities. As a consequence, empirical relationships, dominated by data from better-studied coastal systems or species, are often used to fill in for missing rate measurements or to estimate rates from more readily collected data, like biomass. One example would be the use of relationships based on animal size and temperature (e.g. Ikeda 1985) to compute 'active flux' contributions to carbon export from the daytime metabolic rates of migrating zooplankton (Dam et al. 1995a, Al Mutairi & Landry 2001, Putzeys & Hernández-León 2005,

*Corresponding author: mlandry@ucsd.edu

Hannides et al. 2009, Stukel et al. 2013a, Isla et al. 2015). Biomass-scaled metabolic relationships have also been widely applied to evaluate the adequacy of measured feeding rates for meeting minimum respiratory requirements (Zhang et al. 1995, Calbet et al. 2009), to parametrize metabolic rates in marine ecosystem models (Townsend et al. 1994, Stock & Dunne 2010), to determine carbon demand in the mesopelagic environment (Steinberg et al. 2008), and to estimate zooplankton respiration for the global ocean (Hernández-León & Ikeda 2005). Additionally, empirical growth rate functions (Hirst & Sheader 1997, Hirst & Lampitt 1998, Hirst & Bunker 2003) used in conjunction with the respiration relationships of Ikeda (1985) have provided estimates of community production and full carbon budgets for mesozooplankton in a variety of open-ocean ecosystems, including the Arabian Sea, the equatorial Pacific, the Hawaii and Bermuda time-series stations in the subtropical Pacific and Atlantic Oceans (Roman et al. 2000, 2002a,b), as well as in global ecosystem models (Stock & Dunne 2010). Whether and how zooplankton communities can reasonably function at levels implied by the empirical relationships, however, has not been adequately investigated.

Because temperature has a large effect on the calculated rates from empirical relationships, they predict especially high levels of zooplankton consumption, metabolism, and growth in warm-water tropical and subtropical regions—the very kinds of systems where nutritional deficiency and food-limited growth are otherwise thought to be most significant (Huntley & Boyd 1984, Hopcroft et al. 1998b, Calbet & Agusti 1999, Ward et al. 2012). The case of the equatorial Pacific is typical of the tensions between these contradictory perspectives. In the 1992 US Joint Global Ocean Flux Study in the equatorial Pacific (JGOFS EqPac), Dam et al. (1995b) and Zhang et al. (1995) found that estimates of zooplankton herbivory based on gut fluorescence were not able to satisfy even the respiratory requirements of mesozooplankton computed from the Ikeda (1985) equations. Nonetheless, based on crude estimates of the amount of production that might be available indirectly by feeding on protistan microzooplankton, Dam et al. (1995b) hypothesized that it would be sufficient to support a healthy mesozooplankton community. We take that idea further in the present study using empirical relationships to predict the magnitudes of both respiration and production expected for mesozooplankton in equatorial waters and comparing them to the independent solutions of a food-web inverse model that is tightly constrained by field rate measurements of production and grazing, but does not consider the variables (organism size, temperature, chlorophyll) in the predictive relationships. Our overall hypotheses were that (1) predicted respiration and production rates are supported within the network flows of a balanced steady-state food web and (2) the dietary requirements of mesozooplankton in excess of direct herbivory are mainly met by consumption of microzooplankton.

Our results confirm that zooplankton rates consistent with empirical predictions can be readily satisfied by food-web fluxes that also reproduce many of the previously determined rate relationships for the equatorial Pacific. However, while predation on microzooplankton is the largest component of mesozooplankton diet, it is not the only explanation for how they can achieve high growth. Details of the model are also important in revealing the extent of carbon cycling within the network, efficiency estimates at each step, and the contributions of different pathways to carbon export. Comparisons of our results to food-web properties in the subtropical Pacific at Stn ALOHA provide additional insights into how the nutritional requirements of zooplankton can be met in more oligotrophic waters than the equatorial Pacific and how different components of export could contribute to satisfying mesopelagic carbon demand.

2. MATERIALS AND METHODS

2.1. Biomass and experimental rate determinations

Data for the present analysis came from 2 cruises of the Equatorial Biocomplexity project that sampled the region between 4° N–4° S and 110°–140° W in December 2004 (EB04) and September 2005 (EB05) (Nelson & Landry 2011). Over both cruises, 31 stations were sampled in a similar manner to assess size-structured biomass and composition of the plankton community from bacteria to mesozooplankton. Experiments were also conducted daily at each station to determine rates of nutrient uptake, primary production, phytoplankton growth, and grazing by micro- and mesozooplankton. Methods for all measurements are presented in detail elsewhere and are summarized briefly below with data source citations.

Mesozooplankton were collected at mid-day (10:00–14:00 h) and mid-night (22:00–02:30 h) by double-oblique net tows to a mean (±SE) depth of 144 ± 3.6 m with a 1 m^2 ring net equipped with 200 µm Nitex mesh, a General Oceanics flow meter

to record volume filtered, and a Vyper dive computer (Suunto) to record tow depth and duration (Décima et al. 2011). Subsamples of the tows (1/8 splits) were size-fractioned by wet sieving through nested Nitex screens into 5 size classes of 0.2–0.5, 0.5–1, 1–2, 2–5, and >5 mm. One size-fractioned split was concentrated onto pre-weighed 200 µm Nitex filters, rinsed with isotonic ammonium to remove sea salt, and oven dried (60°C) for 24 h for determination of mesozooplankton dry weights (DWs). A replicate size-fractioned split was collected on GF/F filters and analyzed for gut fluorescence (Décima et al. 2011). Mean daily estimates of mesozooplankton grazing on the bulk phytoplankton community were determined from gut phaeopigment contents and the gut throughput estimate of 2.1 h^{-1} for equatorial zooplankton from Zhang et al. (1995).

Biomass and rate estimates for bacteria and protists at each station are from water collected from CTD-rosette hydrocasts at 8 light depths spanning the euphotic zone. *Prochlorococcus*, *Synechococcus*, and heterotrophic bacteria were enumerated by flow cytometry and converted to carbon estimates based on fixed carbon:cell ratios of 32, 101, and 11 fg C $cell^{-1}$, respectively (Taylor et al. 2011). Protistan phototrophs (plastidic) and heterotrophs (non-pigmented) were enumerated into various categories (diatoms, prymnesiophytes, dinoflagellates, unidentified flagellates), sized by epifluorescence microscopy, and converted to carbon biomass using the equations of Menden-Deuer & Lessard (2000). Ciliates were analyzed separately by inverted microscopy of acid Lugol's preserved settled samples, using the carbon:volume conversions of Putt & Stoecker (1989) and Verity & Langdon (1984) for naked and loricate cells, respectively.

Primary production rates were determined by the standard ^{14}C uptake method in samples incubated for 24 h in calibrated seawater-cooled deck incubators at the same relative light level as the depth of collection (Balch et al. 2011). The *f*-ratio estimates of new production were computed from uptake rates of ^{15}N-labelled NH_4 and NO_3 for 6 h incubations from sunrise to local noon and corrected to daily rates according to McCarthy et al. (1996) and Parker et al. (2011). Parallel measurements of phytoplankton growth and microzooplankton grazing rates were made by the 2 point dilution method in 24 h experiments under the same incubator–light conditions as ^{14}C and ^{15}N uptake experiments (Selph et al. 2011, Landry et al. 2011b). While the microzooplankton assemblage also includes small (<0.2 mm) metazoans, here we associated microzooplankton grazing with the major role of protists. Taxon-specific rates were determined by HPLC pigment analysis (divinyl chlorophyll a [chl *a*] was representative of *Prochlorococcus*, fucoxanthin of DIA, and monovinyl chl *a* of total eukaryotic phytoplankton) and flow cytometry (*Prochlorococcus* and *Synechococcus*). Pigment-derived rates were corrected for systematic changes in cellular pigment content during incubation using the initial and final experimental samples to assess changes in the mean ratios of accessory pigment to microscopical assessments of phytoplankton biomass (e.g. fucoxanthin:diatom carbon). Taxon-specific estimates of net primary production (NPP) were determined from specific growth rates and carbon biomass according to Landry et al. (2000) and integrated for the euphotic zone (Landry et al. 2011a).

2.2. Mesozooplankton respiration and growth rates

We calculated predicted rates of respiration, growth, and production of mesozooplankton from published, empirically derived relationships. For these calculations, DW estimates from the 58 size-fractioned zooplankton tows were first converted to carbon equivalents using the carbon:DW relationships in Landry et al. (2001), which range narrowly from 0.35–0.38 for <5 mm size fractions and are slightly lower (0.32) for >5 mm animals. Day and night tows were then averaged to give mean euphotic-zone carbon values for each station, reflecting the 12 h daylight period at the equator. For the few stations where only daytime net tows were taken, station biomass values were computed using the average night–day biomass ratios for each size class from the other stations.

Respiration rates (RO, µl O_2 $organism^{-1}$ h^{-1}) were computed from estimates of individual body carbon (BC) and environmental temperature (*T*, °C) according to Ikeda (1985):

$$\ln(\mathrm{RO}) = 0.8354 \times \ln(\mathrm{BC,\ mg\ C\ ind.^{-1}}) + 0.0601 \times T + 0.5254 \quad (1)$$

Oxygen utilization rates were converted to respiratory carbon equivalents (RC, µg C $ind.^{-1}$ d^{-1}) by the equation RC = RO × RQ × 24 × 12 / 22.4, where the respiratory quotient (RQ) is assumed to be 0.8 (protein based), 24 converts hourly to daily rates, 12 is the molecular weight of carbon, and 22.4 is the molar volume of an idealized gas at standard temperature and pressure. For the mean BC of individual animals in the 0.2–0.5, 0.5–1, 1–2, 2–5, and >5 mm components of the size-fractioned zooplankton samples, we used estimates of 0.0024, 0.0064, 0.038, 0.117, and 1.90 mg

C animal^{-1}, respectively, determined from measured size-fractioned abundances and carbon biomass in 144 net tows from the subtropical Pacific (Landry et al. 2001). For temperature, we used mean measured values at each station integrated to the depth of the 1% light level (78 ± 11 m), which varied from 22.4–26.2°C (mean ± SD: 24.4 ± 1.1°C). Total community respiration was computed as the sum of all size fractions.

Mesozooplankton production estimates were computed from the growth rate equations of Hirst & Sheader (1997), Hirst & Lampitt (1998), and Hirst & Bunker (2003). The Hirst & Sheader (1997) relationship considers growth rates (G, d^{-1}) of mainly juvenile copepods:

$$\log_{10}(G) = -0.2962 \times \log_{10}(\text{BC, µg C ind.}^{-1}) + 0.0246 \times T - 1.1355 \quad (2)$$

The Hirst & Lampitt (1998) equation includes adults as well as juveniles:

$$\log_{10}(G) = -0.3221 \times \log_{10}(\text{BC, µg C ind.}^{-1}) + 0.0208 \times T - 1.1408 \quad (3)$$

The Hirst & Bunker (2003) relationship considers the effects of food concentration (chl a, µg l^{-1}) in addition to body size and temperature on G of juvenile broadcast spawners:

$$\log_{10}(G) = -0.363 \times \log_{10}(\text{BC, µg C ind}^{-1}) - 0.0143 \times T + 0.135 \times \log_{10}(\text{chl } a) - 0.105 \quad (4)$$

This relationship (Eq. 4) was chosen over the Hirst & Bunker (2003) equation for 'all data' because the latter is heavily dominated (>71%) by adults, which is unrealistic for the open ocean. For all relationships, we first computed specific growth rates based on mean carbon contents of animals in the 5 size fractions and environmental measurements (T, chl a) integrated to the 1% light level. Total zooplankton production was then calculated as the sum of the products of measured biomass and predicted daily rate of biomass increase for each size fraction.

2.3. Analytical framework of the inverse model

As reported by Landry et al. (2011a), the measured stock and rate results from the Equatorial Biocomplexity cruises described a steady-state system in which (1) depth-integrated phytoplankton community production for the euphotic zone was balanced, on average, by grazing losses to combined micro- and mesozooplankton herbivory, (2) carbon-based assessments of phytoplankton production from specific growth rates and microscopical estimates of biomass were consistent with contemporaneous measurements of ^{14}C-primary production, and (3) the contributions to production and grazing processes could be resolved for major phytoplankton groups. The resulting data set of measured variables (Table 1) is therefore unusually detailed and well constrained for exploring unmeasured rates and relationships in the equatorial food web using steady-state inverse analytical techniques.

For the present analysis, we divided the community of phytoplankton (PHY) into 3 functional groups: picocyanobacteria (CYN), diatoms (DIA), and other eukaryotic PHY (AUT). These define populations that were readily distinguished in stock and rate measurements and which were also targeted by distinct groups of grazers (Table 1). In experimentally measured rates, virtually all production of CYN (*Prochlorococcus* and *Synechococcus*) was consumed by protistan grazers, while DIA production was consumed approximately equally by protists and mesozooplankton. The remaining AUTs, including prymnesiophytes, pelagophytes, and biomass-dominant dinoflagellates, had roughly similar grazing losses, with ~60% going to protists and ~40% to mesozooplankton (Landry et al. 2011a).

Bacterial production (BP) and gross primary production (GPP) were not directly measured on our cruises, but both rates were strongly correlated with net ^{14}C-primary production (i.e. NPP) in previous JGOFS work in the region. We therefore used these prior field-derived relationships to set lower and upper bounds of 1.9–2.6 for the ratio of GPP:NPP (Bender et al. 1999) and 0.10–0.22 for the ratio of BP:NPP (Ducklow et al. 1995, Kirchman et al. 1995). Similarly, we used field estimates from the study region to set constraints on particle export from the euphotic zone (5–10% of NPP; Buesseler et al. 1995) and to approximate the contribution of primarily carnivorous species to total metazooplankton biomass (16 ± 1.7%; Le Borgne et al. 2003).

Within the bounds set by field measurements, we allowed carbon to flow among heterotrophic and non-living components of the food web within relatively broad constraints (Fig. 1, Table 2). Four groups or size classes of pelagic consumers were defined. Heterotrophic nanoflagellates (HNF) and microzooplankton (MIC) comprised the protozooplankton (PTZ) and together accounted for the grazing rates measured by the dilution experiments. Suspension-feeding metazooplankton (MES) accounted for herbivory measured by the mesozooplankton gut fluorescence and were fed upon, in turn, by carnivorous metazooplankton (CAR). Total metazooplankton

Table 1. Experimental inputs to the inverse model. Table gives the measured mean rates and biomasses (±95% confidence limits [CLs]) from the EB04 and EB05 cruises. Equations relate the measured rates to the model compartments: diatoms (DIA), other eukaryotic autotrophs (AUT), cyanobacteria (CYN), phytoplankton (PHY = DIA + AUT + CYN), heterotrophic nanoflagellates (HNF), heterotrophic microzooplankton (MIC), protozooplankton (PTZ = HNF + MIC), suspension-feeding mesozooplankton (MES), carnivorous mesozooplankton (CAR), metazooplankton (MTZ = MES + CAR), bacteria (BAC), picodetritus (PDT), nanodetritus (NDT), microdetritus (MDT), detritus (DET = PDT + NDT + MDT), and dissolved organic carbon (DOC). Flows are written as SOURCEtoSINK, from the first carbon pool to the second. gDI, gAU, and gCY: gross primary production of the 3 phytoplankton groups. NPP: net primary production

Rate	Units	Equation	Mean ± 95% CL	Source
DiaNPP	mg C m^{-2} d^{-1}	gDItoDIA – DIAtoRES – DIAtoDOC	156 ± 54	Landry et al. (2011a)
AutNPP	mg C m^{-2} d^{-1}	gAUtoAUT – AUTtoRES – AUTtoDOC	505 ± 95	Landry et al. (2011a)
CynNPP	mg C m^{-2} d^{-1}	gCYtoCYN – CYNtoRES – CYNtoDOC	203 ± 38	Landry et al. (2011a)
DIAtoPTZ	mg C m^{-2} d^{-1}	DIAtoHNF + DIAtoMIC	83 ± 28	Landry et al. (2011a)
AUTtoPTZ	mg C m^{-2} d^{-1}	AUTtoHNF + AUTtoMIC	316 ± 67	Landry et al. (2011a)
CYNtoPTZ	mg C m^{-2} d^{-1}	CYNtoHNF + CYNtoMIC	203 ± 36	Landry et al. (2011a)
PHYtoMES	mg C m^{-2} d^{-1}	DIAtoMES + AUTtoMES	217 ± 41	Décima et al. (2011)
GrazBalance	mg C m^{-2} d^{-1}	NPP(Dia+Aut+Cyn) – PHYtoPTZ – PHYtoMES	–17 ± 60	Landry et al. (2011a)
NewProd		DOCtoEXT + NDTtoEXT + MDTtoEXT + MEStoEXT + CARtoEXT	*f*-ratio × NPP	
Other parameters				
f-ratio			0.22 ± 0.05	Parker et al. (2011)
HNF carbon	mg C m^{-2}		254 ± 39.9	Taylor et al. (2011)
MIC carbon	mg C m^{-2}		297 ± 32.0	Taylor et al. (2011)
MTZ carbon	mg C m^{-2}		994 ± 77	Décima et al. (2011)
BAC carbon	mg C m^{-2}		679 ± 53.5	Parker et al. (2011)
% Carnivores	%		16.0 ± 1.7	Le Borgne et al. (2003)

(MTZ) is the sum of MES and CAR. In addition to PHY, each grazing group was allowed to feed upon smaller consumers (e.g. MIC consume HNF and bacteria [BAC]; MES consume HNF and MIC) as well as appropriately sized detritus. The latter was generated as the fecal egesta from the different sizes of zooplankton (e.g. MIC produce nano-sized detritus [NDT], which can be fed upon by MIC and MES) and by cell death of autotrophs or heterotrophic bacteria (e.g. BAC can die as pico-sized detritus [PDT], which can be consumed by HNF and MIC). MES were not allowed to feed on pico-sized particles, including BAC, CYN, and PDT.

Dissolved organic carbon (DOC) is generated by a variety of processes, including direct production by PHY, viral lysis of bacteria, sloppy feeding and exudation of consumers, and leaching/degradation of detritus. Together, DOC from these pathways supports BP. Energy is dissipated by the respiratory losses (RES) of each living component, by vertical export of detritus from the euphotic zone (allowed only for nano- and microdetritus), by advection of DOC away from the equatorial upwelling zone, and by loss

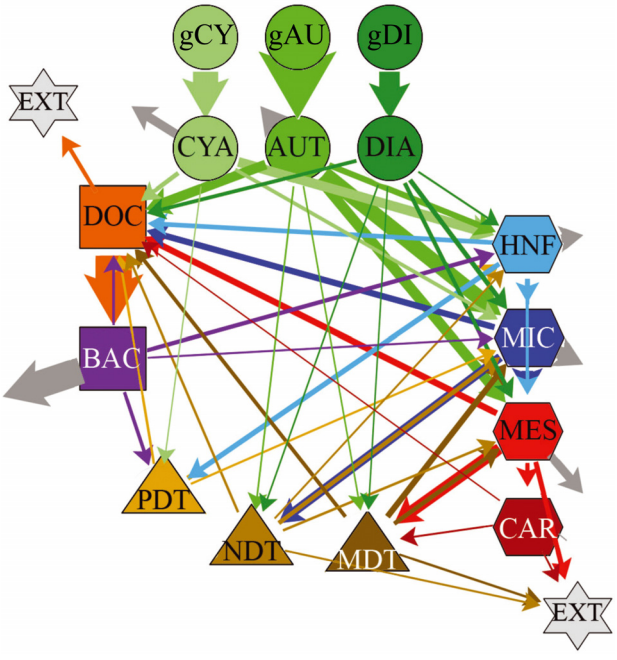

Fig. 1. Equatorial Pacific food web. Dissipation of energy as respiration is shown as unconnected arrows out of each living component. Arrow widths are in proportion to the magnitudes of flows, representing the mean inverse model solution. CYN: cyanobacteria; DIA: diatoms; AUT: other autotrophs; BAC: heterotrophic bacteria; DOC: dissolved organic carbon; HNF: heterotrophic nanoflagellates; MIC: microzooplankton; MES: suspension-feeding mesozooplankton; CAR: carnivorous zooplankton; EXT: export. PDT, NDT, and MDT: pico-, nano-, and micro-sized detritus, respectively. gCY, gAU, and gDI: gross primary production flows of CYN, AUT, and DIA, respectively

of excess metazooplankton production to undetermined higher trophic levels (e.g. higher-order epipelagic consumers or predatory mesopelagics).

Within the modeled trophic network, flows are constrained by (1) a series of steady-state mass balance constraints for each model compartment (**Ex** = **f**), where **E** is a matrix of zeroes, ones, and negative ones determining whether each flow contributes carbon to or removes carbon from a specific compartment, **x** is the vector of ecosystem flows that we wish to constrain, and **f** is a vector of zeroes indicating that the system is at steady state; (2) a set of approximate equalities based on the mean values and uncertainties in actual field measurements of nitrate uptake, PHY growth, and protozoan grazing rates (for each defined functional group), mesozooplankton grazing rates (**Ax** >> *b*; Table 1), where **A** is a matrix that when multiplied by **x** converts modeled ecosystem flows into linear equations that directly map onto our field measurements (values stored in *b*); and (3) a set of inequalities (Gx^3h) that are loosely constrained by upper and lower bounds that reflect realistic constraints on organism physiology or ecological relationships (e.g. constraining gross growth efficiency [GGE] to 10–40%; Table 2). The overall balance constraint for NPP and grazing, NPP(DIA + AUT + CYN) – PHYtoPTZ – PHYtoMES = –17 ± 60 mg C m^{-2} d^{-1} (Table 1), is derived from the euphotic-zone-integrated rate estimates at each station (Landry et al. 2011a) and (as discussed in Section 4.2) plays an important role in returning model solutions with similar mean NPP values and uncertainties as field measurements. For PTZ and MTZ, solutions are allowed within relatively broad bounds of GGE (10–40%) and absorption efficiency (60–90%). For bacteria, we limit losses to DOC to ≤ bacterial losses to grazers, which represents BP returning to colloidal particles via the viral lysis (Fuhrman 1999) of similar magnitude as bacterial mortality to grazers (Fuhrman & Noble 1995). We found it necessary to place an upper limit on this process to avoid unbounded 2-way exchange between BAC and DOC in the network solutions.

Table 2. Minimum and maximum biological constraints on the model solution. GGE: gross growth efficiency; AE: absorption efficiency; BP: bacterial production; NPP: net primary production; GPP: gross primary production; POC: particulate organic carbon. Definitions of planktonic populations as in Table 1

Rate	Population	Minimum	Maximum
GGE	HNF	10%	40%
	MIC	10%	40%
	MES	10%	40%
	CAR	10%	40%
	BAC	5%	30%
AE	HNF	60%	90%
	MIC	60%	90%
	MES	60%	90%
	CAR	60%	90%
Respiration	DIA	10% GPP	55% GPP
	AUT	10% GPP	55% GPP
	CYN	10% GPP	55% GPP
	MES	5% Biomass	20% Biomass
	CAR	2% Biomass	10% Biomass
	BAC	20% Uptake	
Excretion	DIA	2% NPP	55% NPP
	AUT	2% NPP	55% NPP
	CYN	2% NPP	55% NPP
	HNF	10% ingestion	100% respiration
	MIC	10% ingestion	100% respiration
	MES	10% ingestion	100% respiration
	CAR	10% ingestion	100% respiration
	BAC		100% BP
Specific grazing	HNF on DIA		MIC on DIA
	HNF on AUT		MIC on AUT
	HNF on CYN	MIC on CYN	
	HNF on BAC	MIC on BAC	
	HNF on PDT	MIC on PDT	
	HNF on NDT		MIC on NDT
BP	BAC	10% NPP	22% NPP
GPP		190% NPP	260% NPP
POC export		5% NPP	10% NPP

2.4. Inverse model solutions

Inverse ecosystem models are underdetermined systems with more variables (unknown flows to be estimated) than equations (Vézina & Platt 1988, van Oevelen et al. 2010). While our analysis includes more equations (12 mass balance + 9 measured rates = 21 equalities) than many inverse ecosystem constructs, there are 59 flows to determine, and thus an infinite set of vectors that could solve the equalities. To objectively sort through potential solutions, we used the Markov chain Monte Carlo (MCMC) approach of Kones et al. (2009), as implemented in the R code of Van den Meersche et al. (2009). When computing power was more limited, early inverse modeling studies used the L_2 minimum norm approach to determine a unique solution that minimized total ecosystem flows (e.g. Vézina & Platt 1988). Such solutions, however, maximize RES in the lower trophic levels (to achieve minimum flows) and often select extreme values for parameters such as GGE (Niquil et al. 1998, Stukel & Landry 2010). The MCMC approach minimizes those biases and has been shown to recover true ecosystem rates that were withheld

as model inputs (Stukel et al. 2012). The MCMC approach first finds an initial solution that satisfies the inverse problem and then takes a random walk, guided by mass balance constraints and the uncertainties in input measurements, to fully sample the solution space. For our specific system of equations, the Van den Meersche et al. (2009) protocol defines planes bounding the high-dimensional space that can solve the equality and inequality equations ($\mathbf{Ex} = \mathbf{f}$, Gx^3h). We then used the iterative process of selecting a new solution ($\mathbf{x}_n$) set by randomly jumping from a previous solution set ($\mathbf{x}_{n-1}$). For specific implementation details see the mirror algorithm of Van den Meersche et al. (2009). While the new solution always satisfies the exact equalities and inequalities, the decision of whether to accept it or not (and append it to the collection of solution sets) is based on the relative distances of $[\mathbf{Ax}_n - b]$ and $[\mathbf{Ax}_{n-1} - b]$. Specifically, we draw a random number from a uniform distribution from 0–1 and accept the solution if this random number is less than $p(\mathbf{x}_n)/p(\mathbf{x}_{n-1})$, where:

$$p(\mathbf{x}) = e^{-\frac{1}{2}(\mathbf{Ax}-b)^T \mathbf{W}^2 (\mathbf{Ax}-b)} \quad (5)$$

and $\mathbf{W}$ is a weight matrix derived from the uncertainty in each of the field measured variables. This approach thus generates a collection of solution vectors that satisfy the mass balance constraints and inequalities, while approximately solving the measurement equations and taking into account the measurement uncertainties. We determined >800 000 solution vectors. Convergence was tested by comparing the mean of the first 400 000 solution vectors to the mean of the second 400 000 solutions; all variables agreed to within 1%, and most were much closer. The mean of the complete set of all solution vectors is considered the most representative solution to the inverse problem (Kones et al. 2009, Saint-Béat et al. 2013). Confidence limits (CLs; 95%) take into account the uncertainties from both the actual input measurements and the underdeterminacy of the inverse problem.

3. RESULTS

3.1. Calculated rates of mesozooplankton respiration, growth, and production

Table 3 summarizes the details of mesozooplankton rate calculations for the EB04 and EB05 cruises from individual rates to size-class rates to full com-

Table 3. Predicted rates of respiration, growth, and production (means ± 95% confidence limits) for equatorial Pacific zooplankton based on individual carbon content, mean environmental temperature, and chlorophyll *a* concentration (where applicable). Size class carbon estimates for 5 size classes (wet sieved) are the means of day and night net samples at 31 stations (Décima et al. 2011). Individual carbon biomass are size class mean estimates from Landry et al. (2000). Respiration estimates are calculated from the empirical relationships of Ikeda (1985). Growth rate and production calculations are based on equations in Hirst & Sheader (1997), Hirst & Lampitt (1998), and Hirst & Bunker (2003)

	0.2–0.5 mm	0.5–1 mm	1–2 mm	2–5 mm	>5 mm
Total size class (mg C m^{-2})	211 ± 21	248 ± 29	269 ± 36	168 ± 31	64 ± 28
Body carbon (µg C $ind.^{-1}$)	2.4	6.4	38	117	1900
From Ikeda (1985)					
Resp (µg C $ind.^{-1}$ d^{-1})	0.48	1.11	4.88	12.6	129.6
Resp (% body C d^{-1})	20.5 ± 0.4	17.4 ± 0.4	13.0 ± 0.3	10.8 ± 0.2	6.8 ± 0.1
Size class resp (mg C m^{-2} d^{-1})	43.2 ± 4.3	43.5 ± 5.4	35.2 ± 4.7	18.1 ± 3.3	4.4 ± 2.0
TOTAL respiration = 144 ± 16 mg C m^{-2} d^{-1}					
From Hirst & Sheader (1997)					
Specific growth rate (d^{-1})	0.227	0.169	0.100	0.071	0.031
Growth (% body C d^{-1})	25.4 ± 0.6	18.4 ± 0.4	10.5 ± 0.2	7.4 ± 0.2	3.2 ± 0.1
Size class prod (mg C m^{-2} d^{-1})	53.7 ± 5.3	46.1 ± 5.7	28.5 ± 3.8	12.5 ± 2.3	2.0 ± 0.9
TOTAL production = 143 ± 15 mg C m^{-2} d^{-1}					
From Hirst & Lampitt (1998)					
Specific growth rate (d^{-1})	0.177	0.128	0.073	0.050	0.020
Growth (% body C d^{-1})	19.3 ± 0.4	13.7 ± 0.3	7.5 ± 0.1	5.2 ± 0.1	2.1 ± 0.0
Size class prod (mg C m^{-2} d^{-1})	40.8 ± 4.0	34.3 ± 4.2	20.4 ± 2.7	8.7 ± 1.6	1.3 ± 0.6
TOTAL production = 105 ± 11 mg C m^{-2} d^{-1}					
From Hirst & Bunker (2003)					
Specific growth rate (d^{-1})	0.215	0.150	0.079	0.052	0.019
Growth (% body C d^{-1})	24.0 ± 0.4	16.2 ± 0.2	8.2 ± 0.1	5.3 ± 0.1	1.9 ± 0.0
Size class prod (mg C m^{-2} d^{-1})	50.5 ± 5.0	40.2 ± 4.6	22.1 ± 3.0	9.1 ± 1.7	1.2 ± 0.6
TOTAL production = 123 ± 12 mg C m^{-2} d^{-1}					

munity estimates. Since individual rates (e.g. % body C d^{-1}) are computed for animals of a fixed mean size, their small uncertainties account only for variability in the mean environmental parameters (*T*, chl *a*). Uncertainties in rate determinations for size classes and the full zooplankton community additionally account for variability in field-measured biomass.

Among size classes, biomass measurements are highest on average for 1–2 mm zooplankton and drop off sharply for larger sizes (Table 3, Fig. 2). This is at least partially explained by the greater propensity of large zooplankton to migrate out of the euphotic zone during daytime (day:night biomass ratios are 0.40 and 0.11, respectively for the 2–5 and >5 mm fractions, compared to >0.80 on average for <2 mm animals), but it could also reflect some net avoidance. Larger size classes also contribute disproportionally less to the rate estimates. For example, biomass-specific rates of respiration are about 3 fold higher (20.5 vs. 6.8% of body C d^{-1}) for the <0.5 vs. >5 mm size classes, and growth rates are 8–12 times higher for the smaller animals. Individual growth rate predictions from the Hirst & Sheader (1997) equations, ranging from 25 to 3% of body C d^{-1} for the various size fractions, are 30–50% higher than the estimates from Hirst & Lampitt (1998), while the Hirst & Bunker (2003) rates are intermediate.

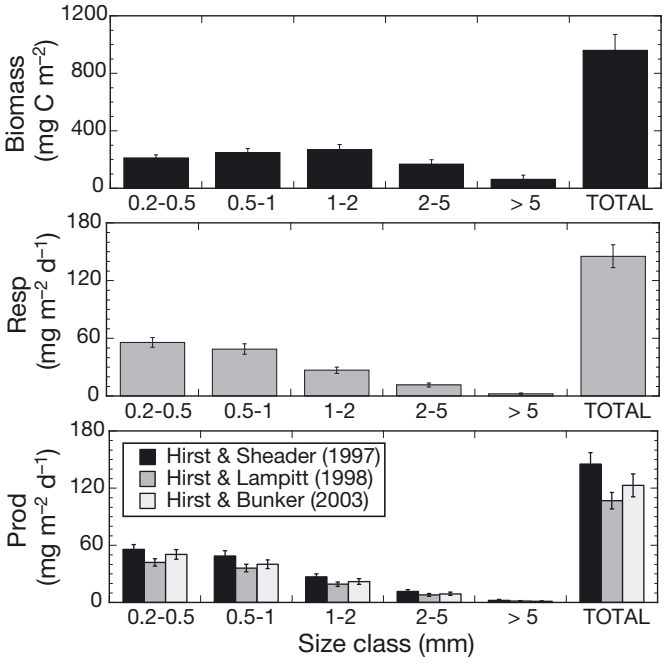

Fig. 2. Size class and community total estimates for mesozooplankton carbon, and respiration and production rates calculated from empirical relationships. Respiration rates are based on Ikeda (1985). Production rates are from 3 growth rate functions as indicated. Error bars: 95% confidence limits

Due to their high biomass-specific rates, <1 mm animals account for 60–74% of the total rate estimates for respiration and production (Table 3, Fig. 2). For the mesozooplankton community as a whole, predicted respiration is 144 ± 16 mg C m^{-2} d^{-1}, while mesozooplankton production estimates vary from 143 ± 15 mg C m^{-2} d^{-1} (Hirst & Sheader 1997) to 105 ± 11 mg C m^{-2} d^{-1} (Hirst & Lampitt 1998).

3.2. Inverse model solutions

The mean values of inverse model solutions for individual carbon flows are depicted by arrow widths in the network connecting sources and sinks in Fig. 2 and listed with their 95% CLs in Table 4. By construct, the distribution of NPP among different categories of PHY and the major trophic flows between PHY and zooplankton are model inputs defined by experimentally determined rates. The model, however, divides the microzooplankton grazing rates from dilution experiments into 2 size groups of protistan consumers, HNF and MIC, and it separates the metazooplankton assemblage (i.e. MTZ) into MES and CAR components, the latter feeding on MES. The remaining (majority of) model solutions relate to unmeasured fluxes, including GPP, DOC, BAC, size-structured detritus, and export, that collectively cycle and dissipate carbon in a manner that maintains a dynamic steady state for food-web productivity and grazing.

While most individual rates cannot be validated, major flux estimates are generally compatible with previously determined rates and relationships for the equatorial Pacific or open ocean. In the model solution, for example, GPP (gDI + gAU + gCY) averages 1.8 times PHY NPP. For the EqPac Program, ^{18}O measurements of gross production corrected for non-carboxylation Mehler and photorespiration reactions give a mean GPP:NPP ratio of 1.9 (Bender et al. 1999). In the model solution, PHY production of DOC (261 mg C m^{-2} d^{-1}) adds 29%, on average, to total NPP particulate production. Comparable data do not exist to our knowledge for the equatorial Pacific, but $DO^{14}C$ production was found to be 22 ± 11% of particulate primary production (mean ± SD, n = 141) for cruises conducted over 2.5 yr period in the subtropical Pacific (Viviani et al. 2015). There is also good agreement between the model ratio of BP to primary production (BP:NPP = 0.136) and the measured ratio from EqPac (0.135; Anderson & Ducklow 2001), and

Table 4. Flux solutions for the inverse trophic model of the equatorial Pacific. Means and 95% confidence limits (CLs) are derived from model runs with randomly drawn input rates derived from field measurements. Definitions and flow conventions (SOURCEtoSINK) are the same as Tables 1 & 2. All rates are mg C m^{-2} d^{-1}

Model flow	Mean rate	95% CL	Model flow	Mean rate	95% CL
gDItoDIA	333	198, 518	MICtoDOC	90	54, 152
DIAtoRES	117	27, 261	MEStoCAR	61	24, 113
DIAtoHNF	21	1, 43	MEStoRES	133	79, 166
DIAtoMIC	66	39, 98	MEStoMDT	182	81, 268
DIAtoMES	56	7, 112	MEStoDOC	95	50, 148
DIAtoNDT	14	0, 45	CARtoRES	13	7, 16
DIAtoMDT	12	0, 39	CARtoMDT	19	4, 43
DIAtoDOC	49	6, 98	CARtoDOC	10	4, 15
gAUtoAUT	870	650, 1106	BACtoHNF	57	15, 112
AUTtoRES	205	78, 438	BACtoMIC	20	1, 54
AUTtoHNF	86	6, 157	BACtoRES	472	323, 650
AUTtoMIC	242	167, 340	BACtoPDT	45	2, 107
AUTtoMES	161	97, 220	BACtoDOC	28	1, 79
AUTtoNDT	15	0, 47	PDTtoHNF	75	15,169
AUTtoMDT	12	0, 41	NDTtoHNF	20	1, 62
AUTtoDOC	149	21, 277	PDTtoMIC	24	1, 71
gCYtoCYN	414	270, 613	NDTtoMIC	64	10, 153
CYNtoRES	139	34, 311	MDTtoMIC	86	4, 211
CYNtoHNF	153	95, 210	NDTtoMES	30	1, 96
CYNtoMIC	49	2, 107	MDTtoMES	61	2, 188
CYNtoPDT	11	0, 34	PDTtoDOC	31	1,96
CYNtoDOC	62	8, 117	NDTtoDOC	29	1, 118
HNFtoMIC	75	4, 169	MDTtoDOC	60	2, 92
HNFtoMES	52	2, 140	DOCtoBAC	603	425, 796
HNFtoRES	144	82, 232	DOCtoEXT	56	2, 145
HNFtoPDT	74	9, 143	NDTtoEXT	21	1, 53
HNFtoDOC	66	35, 116	MDTtoEXT	28	2, 58
MICtoMES	184	69, 303	MEStoEXT	73	6, 155
MICtoRES	217	128, 335	CARtoEXT	19	4, 43
MICtoNDT	136	52, 220			

the model estimate of 20.5% for bacterial growth efficiency is close to the median value of 22% for open-ocean ecosystems (del Giorgio & Cole 1998). Lastly, the model estimate of 49 mg C m^{-2} d^{-1} (5.5% of NPP) for particulate organic carbon (POC) detritus export is within the regional values of 36–60 mg C m^{-2} d^{-1} for the 4° S–4° N latitudinal band from EqPac (Buesseler et al. 1995). Nonetheless, Quay (1997) indicated that a true carbon balance during normal upwelling conditions in the region could require a substantially higher total mean export of ~240 mg C m^{-2} d^{-1}. While we defer full consideration of the model's implications for export to Section 4.4, we note here that the model solutions for export to POC, DOC, and excess zooplankton (MES + CAR) production add up to 197 mg C m^{-2} d^{-1}, without including active flux by vertically migrating zooplankton.

Table 5 provides additional model solutions for aggregate fluxes that combine 2 or more related arrows in Fig. 1 and for fluxes tracked through the network to calculate growth efficiencies and trophic positions (TPs). In general, the uncertainties for aggregate fluxes are substantially smaller than the individual fluxes comprising the aggregates. For example, the 95% CLs for total protozoan grazing on PHY are ±11% of the mean rate (582 ± 68 mg C m^{-2} d^{-1}) compared to uncertainties of ±40–117% of mean estimates for the individual estimates of 2 sizes of grazers (HNF, MIC) feeding on 3 PHY types (DIA, AUT, CYN). To meet aggregate constraints, extreme values for individual fluxes thus appear to be compensated by more moderate related fluxes in the interdependent solution space. Most uncertainties are not symmetrical around solution means because they are determined by the lowest and highest 20 000 solutions (±2.5%) rather than fit to a specific error distribution (e.g. normal curve).

Mean rates of metazooplankton respiration and production from the model aggregate solutions agree closely with the independent values calculated from temperature and biomass distributions, but the CLs are broad compared to calculated estimates. For instance, the model and calculated results for respiration (146 vs. 144 mg C m^{-2} d^{-1}) are almost identical,

Table 5. Aggregate flux and efficiency solutions for the inverse trophic model of the equatorial Pacific. Aggregate fluxes (means and 95% confidence limits [CLs]) are composites for groups (phytoplankton, protozooplankton, metazooplankton, and detritus) with more than one input or output. All rates are mg C m^{-2} d^{-1}. Definitions and flow conventions (SOURCEtoSINK) are the same as Tables 1 & 2; TP: trophic position

Aggregate flux	Mean	95% CL
Phytoplankton GPP	1618	1384, 1742
Phytoplankton NPP	896	825, 966
PHYtoRES	461	254, 659
PHYtoDOC	261	121, 401
PHYtoDET	63	28, 104
PHYtoPTZ	617	551, 682
PHYtoMES	216	178, 255
Bacterial production	122	78, 147
BACtoPTZ	77	23, 131
Protozooplankton production	311	172, 457
PTZtoRES	361	258, 481
PTZtoDOC	156	106, 226
PTZtoDET	210	102, 322
PTZtoMET	236	111, 364
Metazooplankton production	153	72, 241
MTZtoRES	146	92, 179
MTZtoDOC	104	59, 158
MTZtoDET	201	99, 293
MTZtoEXT – higher consumers	92	26, 170
DETtoPTZ	270	110, 473
DETtoMTZ	91	13, 224
DETtoEXT – POC export	49	34, 66
DOCtoEXT – DOC export	56	2, 145
Net PTZtoDET	15	−125, 141
Net MTZtoDET	110	8, 210
Bacteria GGE (%)	20.5	13.4, 27.4
Protozooplankton GGE (%)	29.7	18.5, 38.3
Metazooplankton GGE (%)	25.2	13.5, 37.0
TP protistan nano-grazers (HNF)	2.14	2.04, 2.28
TP protistan micro-grazers (MIC)	2.17	2.03, 2.33
TP mesozooplankton grazers (MES)	2.50	2.29, 2.68
TP carnivorous zooplankton (CAR)	3.50	3.29, 3.68

but values from 92–179 mg C m^{-2} d^{-1} also fit within the 95% CLs for the model rates. Similarly, the model estimate for metazooplankton production (153 mg C m^{-2} d^{-1}) is closest to the 144 mg C m^{-2} d^{-1} calculated from the Hirst & Sheader (1997) equation, but calculated rates from Hirst & Lampitt (1998) and Hirst & Bunker (2003) also lie comfortably within the 95% CLs of 72–241 mg C m^{-2} d^{-1}. Growth efficiencies (lower, upper CL) from the model are 29.7% (18, 38) for protistan consumers and 25% (13, 37) for metazoans (Table 5). Assuming that PHY occupy TP 1.0 and BAC are TP 2.0, network flows indicate that TPs of protists HNF and MIC are virtually the same (2.14–2.17 ± 0.1) while the TP for MES (2.5 ± 0.2) is only about one-third of a level higher.

4. DISCUSSION

One general conclusion that we can make from the inverse model results is that high rates of mesozooplankton respiration, growth, and production, consistent with predictions from the empirical relationships, are realistic within the trophic flows of a natural open-ocean food web. In fact, our mean model solutions for respiration and growth slightly exceed the predictions of Ikeda (1985) and Hirst & Sheader (1997) by a few (1–7%) percent. This level of agreement is particularly notable because the empirical relationships use information only for temperature and size-structured biomass while the model is independently driven by field-measured rates and uncertainties. It is also true, however, that the relatively broad uncertainties of the model solutions are compatible with substantially higher or lower rate predictions. We therefore cannot definitively exclude the lower growth rate and production predictions of Hirst & Lampitt (1998) and Hirst & Bunker (2003) from also being consistent with the model results. What the inverse model provides, more importantly, is a means to explore the network of largely unmeasurable flows that can explain and support high mesozooplankton activity in the open ocean, including where nutrition comes from, where products go, and the implications for trophic structure and efficiencies. In the discussion sections below, we first consider issues relating to model structure and biases. We then synthesize the solution flows going into and out of zooplankton groups and make some comparisons to relative production and trophic structure in more oligotrophic waters of the subtropical Pacific. Finally, we ask how the model export results relate to previous estimates of the requirements for biogeochemical balance in the region and what insights they might provide for meeting mesopelagic carbon demand.

4.1. Inverse model structure and sensitivity

Experimental results from the EB cruises define a steady-state system in which measured PHY production and grazing are closely balanced and measured rate variability is relatively low among widely dispersed stations (Landry et al. 2011a). These characteristics fit what various authors have described as the general chemostat-like quality of the equatorial Pacific region (Frost & Franzen 1992, Landry et al. 1997, Dugdale & Wilkerson 1998) and provide ideal circumstances for assessing ecosystem flows by an

inverse approach with tight data constraints. A previous inverse analysis of EqPac results challenged this view by claiming that a large portion of primary production was left ungrazed (Richardson et al. 2004). In contrast, the EqPac field data upon which the model was based indicated that almost all primary production was consumed by microzooplankton (Verity et al. 1996). As noted by Stukel & Landry (2010), the data–model discrepancy comes from a manipulation of the field estimates of PHY growth rate estimates, which are increased for the model, without increasing microzooplankton grazing by a comparable amount to maintain the observed relationship between grazing and growth. Results of the Richardson et al. (2004) study are thus an artefact of this data management error. The relative success of the current inverse analysis effort can be reasonably judged by the agreement of model solutions with previously established ecosystem relationships for GPP:NPP, DOC:NPP, BP:NPP, bacterial growth efficiency (BGE) and particle export, all well within measurement uncertainties. This does not mean, however, that all fluxes are adequately represented or accurately solved.

There are many ways in which the model structure could be more realistic. Among zooplankton trophic interactions, for instance, the model does not allow feeding of MES on pico-sized particles (CYN, BAC, PDT), thus ignoring short-circuiting of the microbial food web by pelagic tunicates such as appendicularians (Scheinberg et al. 2005), particle-attached bacteria as a potential food resource (Alldredge & Youngbluth 1985), and direct observations and measurements of *Synechococcus* consumption by crustacean zooplankton (Stukel et al. 2013b). There is no component that generates large aggregates from collisions of smaller particles (Burd & Jackson 2009), nor does it allow zooplankton to alter, other than by consumption of whole particles, detrital size structure in ways that might stimulate microbial activity, enhance small particle availability to smaller grazers, or alter export (Mayor et al. 2014). Particle-feeding MES are not allowed to feed carnivorously, though most are functional omnivores that would naturally include eggs, nauplii, and juvenile stages and adults of smaller species in their mixed diet. TPs of MES and CAR are therefore likely underestimates. Viruses are also not explicitly included in the model, although the provisions that allow bacteria to produce DOC and small detrital particles (i.e. PDT) simulate such losses to some extent. While network linkages could be expanded to account for such factors, they would be unconstrained by field measurements and consequently add further to model underdeterminancy and solution uncertainties. We thus believe that the model structure strikes a reasonable balance between simplicity and complexity in representing major flows that are relevant for addressing our particular study questions.

While no systematic effort was made to tune the model to produce specific results or to explore its sensitivity to altered structure or constraints, several runs with different constraints and the same model structure allow us to evaluate sensitivity to varying NPP solutions. An early version of the model (Stukel & Landry 2010) also provides comparative results for a substantially altered model structure. In the absence of a carnivorous zooplankton component (i.e. CAR) and with 2 detrital size classes rather than 3 (e.g. the ECO RW model; Stukel & Landry 2010), MES respiration was substantially higher on average, 179 (97, 294) mg C m^{-2} d^{-1}, than our present model solution, and MES production was lower, 94 (47, 161) mg C m^{-2} d^{-1}. While the 95% CLs for both flux solutions still broadly overlap with those from the current model, the differences in mean solution values indicate that a carnivorous zooplankton component is important in the model structure to diversify nutritional flows so that the entire community does not depend entirely on PHY and protists. Reducing the detrital size classes from 2 to 1 more dramatically impacts the no-CAR model (ECO MC; Stukel & Landry 2010), with solutions for MES respiration (259 [226, 299] mg C m^{-2} d^{-1}) and production (39 [34, 50] mg C m^{-2} d^{-1}) that no longer overlap with current model uncertainties. This pronounced sensitivity indicates that the many functions of detritus as a repository of fecal debris, potential food resource for protists and metazoans, and contributor to export cannot be realistically combined in a single unstructured pool.

In contrast to the strong effects of model structure, solution sensitivity to NPP variability is much reduced. In a model run with the current model structure but without a constraint reflecting the measured growth–grazing balance (GrazBalance in Table 1), group-specific NPP solutions for all PHY were near the upper 95% CLs for the field-measured rates. This reflects a known bias of the MCMC approach, which tends to overestimate NPP and total system energy flow (Stukel et al. 2018). We attempted to minimize this bias in subsequent runs by adding constraints for total measured NPP, for the maximum observed station differential between NPP and grazing, and finally for the overall balance of NPP and grazing, -17 ± 60 mg C m^{-2} d^{-1} (Table 1). We adopted the lat-

ter explicit balance constraint for our model because it generated model solutions closest to measured NPP rate estimates and error distributions. In the testing process, however, different runs with constraints added individually or in combination gave mean NPP solutions that varied from 788–974 mg C m^{-2} d^{-1}, which we use as the basis for sensitivity observations. Despite NPP variability, MES respiration and production rates ranged narrowly from 139–147 and 142–155 mg C m^{-2} d^{-1}, respectively, among runs. Growth efficiency estimates were similarly stable (BGE = 19.7–21.6%; PTZ GGE = 28.4–31.0%; MES GGE = 25.2–25.4%). Thus, for our given model structure, the network analysis provided robust solutions even when challenged by NPP values at the upper and lower limits of field-measured rates.

4.2. Zooplankton dietary sources, sinks, and efficiencies

In discussing results from the JGOFS EqPac study, Dam et al. (1995b) observed that direct mesozooplankton herbivory fell far short of satisfying respiration and growth requirements and sought to resolve this deficit with feeding on other sources. The main hypothesis for the present analysis derives from their initial crude grazing budget suggesting that predation on protistan microzooplankton could be sufficient. As described in more detail below, our analysis strongly supports a major contribution of PTZ to mesozooplankton diets, but also points to smaller but important contributions of other nutritional sources (detritus, carnivory), that were mentioned but not explicitly considered by Dam et al. (1995b). However, our measurements of mesozooplankton biomass and herbivory for the EB cruises were ~2 times higher than during EqPac (Décima et al. 2011), while NPP was lower than the EqPac average of 1140 mg C m^{-2} d^{-1} reported by Barber et al. (1996). Our results thus do not represent the specific circumstances of food-web structure and flows during EqPac, but rather those that occurred at a time when the ratio of zooplankton biomass supported by NPP was higher than EqPac.

Model solutions for the input and output fluxes to aggregate proto- (PTZ = HNF + MIC) and metazooplankton (MTZ = MES + CAR) are summarized in Fig. 3. PHY dominates the dietary input of PTZ (59%), with rates that come directly from experimental measurements. Heterotrophic BAC comprise a relatively small component of total dietary input

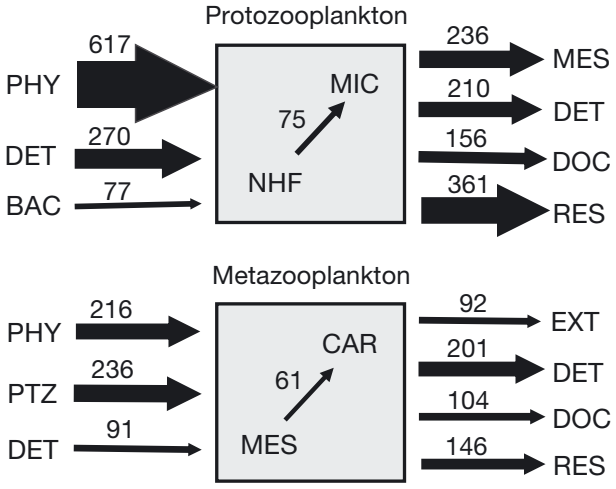

Fig. 3. Aggregate carbon flows into and out of protozooplankton (PTZ: heterotrophic nanoflagellates [HNF] + microzooplankton [MIC]) and metazooplankton (MTZ: suspension-feeding [MES] + carnivorous mesozooplankton [CAR]). All flows are mean model solutions given as mg C m^{-2} d^{-1} integrated for the euphotic zone. PHY: phytoplankton (sum of flows from cyanobacteria, other autotrophs, and diatoms); DET: detritus (sum of flows from pico-, nano-, and micro-sized detritus); BAC: bacteria; DOC: dissolved organic carbon; RES: respiration; EXT: export

(7%), while consumption of small detritus is more significant (26%). This latter result might arise because we did not allow PDT to sink as particle export or to be consumed by BAC or MES; it thus had only 2 outlets: dissolution to DOC or consumption by protists. Nonetheless, as protists readily consume small inert particles or heat-killed prey (Børsheim 1984, Sherr et al. 1987), the role of fine non-living particulates as a nutritional supplement is not unreasonable. Grazing also makes PTZ essentially neutral with regard to net production/consumption of detritus in the food web (net PTZtoDET = 15 [−125, 141] mg C m^{-2} d^{-1} is not significantly different from zero; Table 5). Consumption of HNF production by larger MIC protists (HNFtoMIC = 75 mg C m^{-2} d^{-1}) is portrayed in Fig. 3 as a trophic interaction within the PTZ guild and contributes equally to total dietary intake and to total production of PTZ. The majority of PTZ production (236 mg C m^{-2} d^{-1}; 76% of the total), however, is available for consumption by MES.

Consumption of PTZ comprises the largest dietary resource for MTZ, slightly more than direct utilization of PHY but 2.6 times greater than the model solution for feeding on detritus. Predation on suspension feeders by planktonic carnivores (MEStoCAR) utilizes 40% of MTZ production (153 mg C m^{-2} d^{-1}), with the remainder exported/available (EXT) to

higher-order predators, which are not explicitly included in the model but are considered further in Section 4.3 below.

Calbet & Landry (2004) suggested that heterotrophic protists respire 35–60% of particulate NPP in the global ocean, the broad range reflecting different assumptions about the number of protistan food-web steps. Compared on that same basis in the present analysis (i.e. ignoring PHY production of DOC), equatorial Pacific PTZ respire 40% of NPP. This is roughly what would be expected for a food web in which 70% of PHY production is consumed by protists that reside, on average, only slightly more than one full trophic level above PHY (TP = 2.14–2.17; Table 5), on the lower end of the Calbet & Landry (2004) range. MTZ respiration (16% of NPP) is less than half that of PTZ. Consistent with experimentally derived estimates for the open ocean, including the equatorial Pacific (Anderson & Ducklow 2001), BAC account for the largest portion (51%) of NPP loss to respiration.

Together, PTZ and MTZ provide 43% of the total DOC required to support BP in our network solutions, the same percentage that comes from PHY production of DOC. The remainder derives from microbially associated processes (detrital dissolution, viral lysis of bacteria). Since all of these processes are difficult to quantify and clearly distinguish in field experiments, these results mainly reinforce the general view that pathways to DOC are broadly distributed within plankton food webs (Azam et al. 1983, Jumars et al. 1989, Strom et al. 1997, Marañón et al. 2004).

The mean model solution for GGE of PTZ (29.7%, 18.5–38.3% CL) is consistent with the published values summarized by Straile (1997), and the mean value (30%) that has been used to extrapolate microzooplankton consumption of PHY into global estimates of PTZ contributions to ocean respiration (Calbet & Landry 2004), carbon production (Landry & Calbet 2004), and general food-web fluxes (Steinberg & Landry 2017). The estimated GGE for MTZ (25.2%, 13.5–37.0% CL) also agrees well with published values (copepod mean GGE = 26%; Straile 1997) and seems intuitively reasonable for animals that are respiring and growing at rates close to those predicted by general energetic and growth relationships. Nonetheless, this efficiency is slightly lower than the 30% assumed in synthesis studies (e.g. Roman et al. 2002a,b) that have back-calculated ingestion rates from estimates of zooplankton production based on the Hirst & Lampitt (1998) equation.

4.3. Meeting mesozooplankton carbon requirements

The good agreement between modeled and predicted rates of zooplankton respiration and growth for the equatorial Pacific illustrates how bulk nutritional requirements can be met within the framework of a tightly constrained food-web network. How this relates to the concept of zooplankton food limitation in the open oceans is complicated by the fact that the empirical relationships represent average, not maximum, rates for relatively few species and may not fully capture those populations at food excess conditions. Bottle experiments to study feeding of open-ocean zooplankton also do not reproduce the conditions of patchiness, particle size distributions, and chemical cues that zooplankton experience during natural free swimming and feeding in the ambient water column. We do, however, observe that the Hirst & Bunker (2003) function, which uses environmental chl *a* to account explicitly for food limitation, fits the mean model solution for MTZ production less well, though still adequate statistically, compared to the Hirst & Sheader (1997) function. Chl *a* may therefore be less reliable as an indicator of zooplankton food resources in the open ocean, where there is generally less dependence on direct herbivory. We used the Hirst & Bunker (2003) equation for the juveniles of broadcast spawners for our production predictions because it gave the highest growth rate estimates compared to the equation that included egg sac carriers and mainly slow-growing copepod adults. For the sake of comparison, the Hirst & Bunker (2003) 'all data' regression predicts a rate of 48 ± 5 mg C m^{-2} d^{-1} for food-limited mesozooplankton in our study region, which is only about one-third of the estimate for juvenile spawners and well below the lower CL for our model production estimate. Similarly, the low growth estimates from Hirst & Lampitt (1998) mainly reflect adult animals. Under field conditions, where adult longevity may be relatively short, the rates for juvenile growth more likely reflect the potential, if not the realized average, for the community. The present results indicate that the Hirst & Sheader (1997) equation is a realistic indicator of that potential for open-ocean zooplankton.

Another issue that must be considered in using empirical relationships is how they apply to the community being examined. Here, we used growth rate equations based entirely on copepods to predict rates for a more diverse zooplankton assemblage. While it can be argued that some taxa grow slower than copepods of the same size, other taxa, like appendicularian-

ans, have substantially higher feeding and growth rate potentials (Alldredge 1981, Hopcroft et al. 1998a). The net effect on bias, if any, in the empirical relationships is not clear. For similar size-fractionation to that in the present study, copepods (~80%) and appendicularians (~10%) overwhelmingly dominate zooplankton abundances of the subtropical Pacific (Landry et al. 2001), particularly in the smaller size fractions that contribute disproportionately to our zooplankton production estimates (Fig. 2). While not perfect, therefore, the relative importance of copepod-dominated size classes in the production calculations provides a reasonable justification for using the copepod-based growth relationships for the community in general in our analyses.

Equatorial regions typically have higher mean chl *a*, primary production, and zooplankton biomass compared to adjacent subtropical gyres (Isla et al. 2004, Behrenfeld et al. 2005, Moriarty et al. 2013). Whether reduced productivity of oligotrophic subtropical regions could also support high levels of zooplankton respiration and growth similar to the equatorial Pacific is a reasonable question to ask, and, if so, how might that scale relative to the present results? Based on long-term data (1994–2013) from Stn ALOHA, Valencia et al. (2018) determined that mesozooplankton in the subtropical North Pacific could meet the requirements of the Ikeda (1985) and Hirst & Sheader (1997) rate equations if they consumed the equivalent of 34% of primary production. In relative terms, this is only half the rate of MTZ carbon ingestion (604 mg C m^{-2} d^{-1} = 67% of NPP; Table 5) that we find to be realistic for food web fluxes in the equatorial Pacific. Part of the difference can be explained by the warmer (1–2°C) euphotic zone temperature of the equatorial region, but most is likely linked to the greater dominance of picophytoplankton as primary producers in the subtropics, which reduces trophic transfer efficiency to support zooplankton. Indeed, Valencia et al. (2018) concluded that the consumption requirements for respiration and growth at Stn ALOHA were consistent with projected flows through the trophic structure of that region, which includes almost a full trophic level for protistan MIC, on average, between primary producers and mesozooplankton (Landry & Décima 2017). Based on the comparison of these 2 systems, empirical relationships for respiration and growth might broadly be useful for predicting the steady-state levels of mesozooplankton biomass supported by primary production in the open oceans, including the oligotrophic subtropics, but would need to account for regional variability in trophic structure.

4.4. Total export and implications for mesopelagic carbon demand

Resolving the complex interplay of biological interactions and biogeochemical processes in the mesopelagic 'twilight zone' is a major contemporary challenge for understanding carbon cycling in the oceans (Robinson et al. 2010). One first-order question is reconciling how export fluxes from the euphotic zone might meet carbon demand in the mesopelagic layer where most export is utilized. Steinberg et al. (2008), for instance, documented striking disparities between sinking POC export and the carbon demands of mesopelagic bacteria and zooplankton in the subtropical and subarctic North Pacific, and speculated that predatory losses of mesozooplankton to mesopelagic consumers could be an important unmeasured term for closing the gap. Our model results are relevant to this discussion because they provide food-web constrained estimates of the various components that contribute to total export, including the availability of excess MTZ production to satisfy mesopelagic carbon demand.

Two elements are missing, however, from our analysis: (1) mesopelagic carbon demand for the equatorial Pacific, and (2) and the component of total carbon exported as respiration and organic excretion of migratory zooplankton at daytime mesopelagic depths (i.e. active export). As the basis for discussion, we estimate the former from the Steinberg et al. (2008) results for Stn ALOHA. For low estimates, we use the combined carbon demands of bacteria and mesozooplankton for depth zones of 150–500 and 150–1000 m that were found for Stn ALOHA (Table 6). Our upper estimates are scaled in proportion to the 1.74 greater NPP for the equatorial Pacific (896 mg C m^{-2} d^{-1}) relative to the 2 decade average of 516 mg C m^{-2} d^{-1} for Stn ALOHA (Valencia et al. 2018). Uncertainties in the carbon demand estimates in Table 6 reflect different assumptions for carbon conversions (Steinberg et al. 2008). Active flux estimates for migratory zooplankton are computed as in previous estimates for Stn ALOHA (Al Mutairi & Landry 2001) using the differences between size-fractioned day and nighttime net tows as a measure of migrating biomass, computing daytime RES at 200–500 m depth (mean temperature = 10.5°C) from Eq. (1) in Ikeda (1985), and including an additional 33% of RES to account for DOC excretion. As observed by Steinberg et al. (2008), active export is a modest fraction of passive POC export and contributes little to resolving the disparity between POC export and mesopelagic carbon demand, especially

Table 6. Estimates of mesopelagic carbon demand and export fluxes for the equatorial Pacific. Mesopelagic carbon demands are scaled to estimates for Stn ALOHA from Steinberg et al. (2008). Mean values are the sums of carbon demands for bacteria and zooplankton in mesopelagic depth ranges of 150–500 or 150–1000 m. Parentheses are upper and lower uncertainty estimates due to different assumptions about conversion factors. For export fluxes, particulate organic carbon (POC), dissolved organic carbon (DOC), and metazoan (MTZ) losses to predators are mean values and 95% confidence limits (CLs) from solutions of the inverse trophic model. Active flux is respiration and organic excretion for diel vertical migrators at 200–500 m daytime depth calculated from biomass estimates and Ikeda (1985) equations according to Al Mutairi & Landry (2001). All rates are mg C m^{-2} d^{-1}

Depth range (m)	Mesopelagic carbon demand estimates		Export flux estimates		
	Lower	Upper	Process	Mean	95% CL
150–500	60 (38, 84)	105 (53, 118)	POC sinking	49	34, 66
150–1000	90 (53, 126)	157 (92, 220)	DOC mixing	56	2, 145
			MTZ predation	92	26, 170
			Active flux	15	10, 21
			TOTAL	212	

for the upper demand estimates (Table 6). We thus turn our attention below to the larger model-derived export fluxes for DOC and predation. Overall, however, we note that total export from all mechanisms (215 mg C m^{-2} d^{-1}) is, within estimate uncertainties, close to the ~240 mg C m^{-2} d^{-1} that Quay (1997) determined is needed to balance new production during normal upwelling conditions in the equatorial Pacific. The combined components of export in Table 6 are thus of a magnitude that resolves the general biogeochemical balance for the region.

Archer et al. (1997) argued that maintaining steady-state DOC concentrations in the 3-dimensional circulation of the equatorial Pacific required total DOC production of at least half that of NPP. Our model mean solutions set the total production of DOC from all sources to 669 mg C m^{-2} d^{-1}, or 75% of NPP. CLs for the mean model solution for DOC export (56 mg C m^{-2} d^{-1}) are almost as large as the upper estimates of mesopelagic carbon demand. Nonetheless, the circulation of the region should allow efficient transport of excess DOC to the mesopelagic with strong meridional 2-directional flows that move surface water rapidly away from the divergent upwelling core to subduction fronts, then back again at depth (Walsh et al. 1997). This circulation mechanism could play a significant role in meeting upper mesopelagic bacterial carbon demand for labile DOC across the equatorial belt and might even provide some subsidy to adjacent subtropical regions via isopycnal transport.

Availability of excess MTZ production to predation is the largest term in our export summary (92 mg C m^{-2} d^{-1}) and, as Steinberg et al. (2008) deduced, the most likely process for resolving the deficit in mesopelagic carbon demand that is not met by POC sinking. In the present example, the combination of POC sinking, active flux, and predation would be sufficient to satisfy the upper estimate for 150–1000 m carbon demand, without any DOC contribution. This is likely unrealistic, however, as predation also needs to sustain higher consumers (e.g. flying fish, tunas, and seabirds) of the epipelagic zone that are not considered in our food web. Even so, it is easy to see how the different components of export could collectively meet mesopelagic carbon demand (Table 6). For the predation component specifically, Kelly et al. (2019) suggested that ~40% of predation on MTZ communities occurred in the mesopelagic depth range, based on an inverse analysis of epi- and mesopelagic communities in regions spanning the coastal California Current to the edge of the North Pacific Subtropical Gyre. Scaled to our estimates of total predation, 37 mg C m^{-2} d^{-1} might therefore go to meeting the needs of the diverse resident mesopelagic community that prey upon vertically migrating zooplankton (Robison et al. 2020). Additional predatory loss of epipelagic zooplankton production would also be expected to go to migratory mesopelagics too large or elusive to be sampled by our net tows (therefore not included in our estimates of CAR feeding or active migratory flux). These are details, however, that can only be determined from a focused field study with appropriate methods.

To conclude this discussion, we make 3 points about this export example that tie together the major themes of our study. First, trophic interactions within the epipelagic not only determine elemental cycling and productivity of that zone but also the magnitudes and forms of carbon exported from it. As we have illustrated, inverse analysis of epipelagic food-web fluxes can provide strong constraints on export mechanisms (DOC, excess MTZ production) that would be extremely difficult to quantify from a meso-

pelagic-focused study alone. The present study might therefore provide an example of what minimally needs to be measured in the euphotic zone in order to understand nutritional sources and trophic cycling in the mesopelagic realm. Second, inverse analysis can also be a powerful framework for defining mesopelagic carbon demand as a coherent food-web problem. Here, for the sake of simplicity, we have presented the carbon demands for mesopelagic zooplankton and bacteria as if they were additive. In our trophic model, however, NPP of 896 mg C m^{-2} d^{-1} fully satisfies carbon demands of BAC, PTZ, and MTZ that are much larger (2246 mg C m^{-2} d^{-1}) because the carbon is utilized many times over within the trophic network before being eventually lost as respiration. Careful *a priori* attention to the structure of mesopelagic food webs could thus provide useful insights for recalibrating the magnitude of carbon demand that is not met by POC sinking export and for identifying the specific processes that need to be measured in field studies to resolve mesopelagic carbon sources and uses in an integrated food-web context. Lastly, to the extent that substantial predation on zooplankton is needed to satisfy mesopelagic carbon demand, it supports high growth rates of zooplankton in the open ocean. For example, relying on MTZ predation by mesopelagics to fill the 41 mg C m^{-2} d^{-1} deficit between mesopelagic carbon demand and combined POC and active flux for the 150–500 m depth range at Stn ALOHA, as suggested by Steinberg et al. (2008), implies a sustained daily loss rate of 11.8% of mesozooplankton biomass, which averages 350 mg C m^{-2} in that region (Valencia et al. 2018). Our trophic model yields 9.3% of MTZ standing stock d^{-1} for equatorial zooplankton (994 mg C m^{-2}; Table 1) as excess production to export. Considering that the ALOHA estimate is likely exaggerated because it does not account for mesopelagic trophic cycling but that excess MTZ production in both systems also need to satisfy the requirements of higher epipelagic consumers in addition to resident mesopelagic predation, conclusions from the perspectives of epipelagic food-web cycling and mesopelagic carbon demand are very similar.

Acknowledgements. This project was supported by the National Science Foundation (NSF) grants OCE-0322074 and -1851558 to M.R.L., OCE-1756517 to the Hawaii Ocean Timeseries program, NSF and NASA Earth and Space Science Graduate Research Fellowships to M.R.S., and NIWA COES1901 and COES2001 to M.D. We are deeply indebted to the captain and crew of the R/V 'Revelle', to Chief Scientist David Nelson, and to all of the cruise participants who produced the original data and publications upon which this analysis is based.

LITERATURE CITED

Al-Mutairi H, Landry MR (2001) Active export of carbon and nitrogen at Station ALOHA by diel migrant zooplankton. Deep Sea Res II 48:2083–2104

Alldredge AL (1981) The impact of appendicularian grazing on natural food concentrations *in situ*. Limnol Oceanogr 26:247–257

Alldredge AL, Youngbluth MJ (1985) The significance of macroscopic aggregates as sites for heterotrophic bacterial production in the mesopelagic zone of the subtropical Atlantic. Deep Sea Res A 32:1445–1456

Anderson TR, Ducklow HW (2001) Microbial loop carbon cycling in ocean environments studied using a simple steady-state model. Aquat Microb Ecol 26:37–49

Archer D, Peltzer ET, Kirchman DL (1997) A timescale for dissolved organic carbon production in equatorial Pacific surface waters. Global Biogeochem Cycles 11:435–452

Azam F, Fenchel T, Gray JG, Meyer-Reil LA, Thingstad F (1983) The ecological role of water-column microbes in the sea. Mar Ecol Prog Ser 10:257–263

Balch WM, Poulton AJ, Drapeau DT, Bowler BC, Windecker LA, Booth ES (2011) Zonal and meridional patterns of phytoplankton biomass and carbon fixation in the equatorial Pacific Ocean between 110°W and 140°W. Deep Sea Res II 58:400–416

Barber RT, Sanderson MP, Lindley ST, Chai F and others (1996) Primary productivity and its regulation in the equatorial Pacific during and following the 1991–1992 El Niño. Deep Sea Res II 43:933–969

Behrenfeld MJ, Boss E, Siegel DA, Shea DM (2005) Carbon-based ocean productivity and phytoplankton physiology from space. Global Biogeochem Cycles 19:GB1006

Bender M, Orchardo J, Dickson ML, Barber RT, Lindley S (1999) *In vitro* O_2 fluxes compared with ^{14}C production and other rate terms during the JGOFS equatorial Pacific experiment. Deep Sea Res I 46:637–654

Børsheim KY (1984) Clearance rates of bacteria-sized particles by freshwater ciliates, measured with monodisperse fluorescent latex beads. Oecologia 63:286–288

Buesseler KO, Andrews JA, Hartman MC, Belastock R, Chai F (1995) Regional estimates of the export flux of particulate organic carbon derived from thorium-234 during the JGOFS EqPac program. Deep Sea Res II 42:777–804

Burd AB, Jackson GA (2009) Particle aggregation. Annu Rev Mar Sci 1:65–90

Calbet A, Agusti S (1999) Latitudinal changes in copepod egg production rates in Atlantic waters: temperature and food availability as the main driving factors. Mar Ecol Prog Ser 181:155–162

Calbet A, Landry MR (2004) Phytoplankton growth, microzooplankton grazing and carbon cycling in marine systems. Limnol Oceanogr 49:51–57

Calbet A, Atienza D, Henriksen CI, Saiz E, Adey TR (2009) Zooplankton grazing in the Atlantic Ocean: a latitudinal study. Deep Sea Res II 56:954–963

Dam HG, Roman MR, Youngbluth MJ (1995a) Downward export of respiratory carbon and dissolved inorganic nitrogen by diel-migrant mesozooplankton at the JGOFS Bermuda time-series station. Deep Sea Res I 42: 1187–1197

Dam HG, Zhang X, Butler M, Roman MR (1995b) Mesozooplankton grazing and metabolism at the equator in the central Pacific: implications for carbon and nitrogen fluxes. Deep Sea Res II 42:735–756

Décima M, Landry MR, Rykaczewski RR (2011) Broad scale patterns in mesozooplankton biomass and grazing in the

eastern equatorial Pacific. Deep Sea Res II 58:387–399
del Giorgio PA, Cole JJC (1998) Bacterial growth efficiency in natural aquatic systems. Annu Rev Ecol Syst 29: 503–541
Ducklow HW, Quinby HL, Carlson CA (1995) Bacterioplankton dynamics in the equatorial Pacific during the 1992 El Niño. Deep Sea Res II 42:621–638
Dugdale RC, Wilkerson FP (1998) Silicate regulation of new production in the Equatorial Pacific upwelling. Nature 391:270–273
Frost BW, Franzen NC (1992) Grazing and iron limitation in the control of phytoplankton stock and nutrient concentration: a chemostat analogue of the Pacific equatorial upwelling zone. Mar Ecol Prog Ser 83:291–303
Fuhrman JA (1999) Marine viruses and their biogeochemical and ecological effects. Nature 399:541–548
Fuhrman JA, Noble RT (1995) Viruses and protists cause similar mortality in coastal seawater. Limnol Oceanogr 40:1236–1242
Hannides CCS, Landry MR, Benitez-Nelson CR, Styles RM, Montoya JP, Karl DM (2009) Export stoichiometry and migrant-mediated flux of phosphorus in the North Pacific Subtropical Gyre. Deep Sea Res I 56:73–88
Hernández-León S, Ikeda T (2005) A global assessment of mesozooplankton respiration in the ocean. J Plankton Res 27:153–158
Hirst AG, Bunker AJ (2003) Growth in marine planktonic copepods: global rates and patterns in relation to chlorophyll *a*, temperature, and body weight. Limnol Oceanogr 48:1988–2010
Hirst AG, Lampitt RS (1998) Towards a global model of *in situ* weight-specific growth rates in marine planktonic copepods. Mar Biol 132:247–257
Hirst AG, Sheader M (1997) Are *in situ* weight-specific growth rates body-size independent in marine planktonic copepods? A re-analysis of the global synthesis and a new empirical model. Mar Ecol Prog Ser 154:155–165
Hopcroft RR, Roff JC, Bouman HA (1998a) Zooplankton growth rates: the larvaceans *Appendicularia*, *Fritillaria* and *Oikopleura* in tropical waters. J Plankton Res 20: 539–555
Hopcroft RR, Roff JC, Webber MK, Witt JDS (1998b) Zooplankton growth rates: the influence of size and resources in tropical marine copepodites. Mar Biol 132:67–77
Huntley M, Boyd C (1984) Food-limited growth of marine zooplankton. Am Nat 124:455–478
Ikeda T (1985) Metabolic rates of epipelagic marine zooplankton as a function of body mass and temperature. Mar Biol 85:1–11
Isla JA, Llope M, Anadón R (2004) Size-fractionated mesozooplankton biomass, metabolism and grazing along a 50°N–30°S transect of the Atlantic Ocean. J Plankton Res 26:1301–1313
Isla JA, Scharek R, Latasa M (2015) Zooplankton diel vertical migration and contribution to deep active carbon flux in the NW Mediterranean. J Mar Syst 143:86–97
Jumars PA, Penry DL, Barross JA, Perry MJ, Frost BW (1989) Closing the microbial loop: dissolved carbon pathway from incomplete ingestion, digestion and absorption in animals. Deep Sea Res A 36:483–495
Kelly TB, Davison PR, Goericke R, Landry MR, Ohman MD, Stukel MR (2019) The importance of mesozooplankton diel vertical migration for supporting a mesopelagic ecosystem. Front Mar Sci 6:508
Kirchman DL, Rich JH, Barber RT (1995) Biomass and biomass production of heterotrophic bacteria along 140°W in the equatorial Pacific—effect of temperature on the microbial loop. Deep Sea Res II 42:603–619
Kones JK, Soetaert K, van Oevelen D, Owino JO (2009) Are network indices robust indicators of food web functioning? A Monte Carlo approach. Ecol Model 220:370–382
Landry MR, Calbet A (2004) Microzooplankton production in the oceans. ICES J Mar Sci 61:501–507
Landry MR, Décima MR (2017) Protistan microzooplankton and the trophic position of tuna: quantifying the trophic link between micro- and mesozooplankton in marine foodwebs. ICES J Mar Sci 74:1885–1892
Landry MR, Barber RT, Bidigare RR, Chai F and others (1997) Iron and grazing constraints on primary production in the central equatorial Pacific: an EqPac synthesis. Limnol Oceanogr 42:405–418
Landry MR, Constantinou J, Latasa M, Brown SL, Bidigare RR, Ondrusek ME (2000) Biological response to iron fertilization in the eastern equatorial Pacific (IronEx II). III. Dynamics of phytoplankton growth and microzooplankton grazing. Mar Ecol Prog Ser 201:57–72
Landry MR, Al-Mutairi H, Selph KE, Christensen S, Nunnery S (2001) Seasonal patterns of mesozooplankton abundance and biomass at Station ALOHA. Deep Sea Res II 48:2037–2062
Landry MR, Selph KE, Taylor AG, Décima M, Balch WM, Bidigare RR (2011a) Phytoplankton growth, grazing and production balances in the HNLC equatorial Pacific. Deep Sea Res II 58:524–535
Landry MR, Selph KE, Yang EJ (2011b) Decoupled phytoplankton growth and microzooplankton grazing in the deep euphotic zone of the eastern equatorial Pacific. Mar Ecol Prog Ser 421:13–24
Le Borgne R, Champalbert G, Gaudy R (2003) Mesozooplankton biomass and composition in the equatorial Pacific along 180°. J Geophys Res Oceans 108:8143
Marañón E, Cermeno P, Fernandez E, Rodriguez J, Zabala L (2004) Significance and mechanisms of photosynthetic production of dissolved organic carbon in a coastal eutrophic ecosystem. Limnol Oceanogr 49:1652–1666
Mayor DJ, Sanders R, Giering SLC, Anderson TR (2014) Microbial gardening in the ocean's twilight zone: detritivorous metazoans benefit from fragmenting, rather than ingesting, sinking detritus. BioEssays 36:1132–1137
McCarthy JJ, Garside C, Nevins JL, Barber RT (1996) New production along 140°W in the equatorial Pacific during and following the 1992 El Niño event. Deep Sea Res II 43: 1065–1093
Menden-Deuer S, Lessard EJ (2000) Carbon to volume relationships for dinoflagellates, diatoms, and other protist plankton. Limnol Oceanogr 45:569–579
Moriarty R, Buitenhuis ET, Le Quére C, Gosselin MP (2013) Distribution of known macrozooplankton abundance and biomass in the global ocean. Earth Syst Sci Data 5: 241–257
Nelson DM, Landry MR (2011) Regulation of phytoplankton production and upper-ocean biogeochemistry in the eastern equatorial Pacific: introduction to results of the Equatorial Biocomplexity project. Deep Sea Res II 58: 277–283
Niquil N, Jackson GA, Legendre L, Delesallel B (1998) Inverse model analysis of the planktonic food web of Takapoto Atoll (French Polynesia). Mar Ecol Prog Ser 165:17–29
Parker AE, Wilkerson FP, Dugdale RC, Marchi A, Hogue VE, Landry MR, Taylor AG (2011) Spatial patterns of nitrogen uptake and phytoplankton in the equatorial upwelling zone (110°W–140°W) during 2004 and 2005. Deep Sea Res II 58:417–433

Putt M, Stoecker DK (1989) An experimentally determined carbon: volume ratio for marine 'oligotrichous' ciliates from estuarine and coastal waters. Limnol Oceanogr 34: 1097–1103

Putzeys S, Hernández-León S (2005) A model of zooplankton diel vertical migration off the Canary Islands: implication for active carbon flux. J Sea Res 53:213–222

Quay P (1997) Was a carbon balance measured in the equatorial Pacific during JGOFS? Deep Sea Res II 44: 1765–1781

Richardson TL, Jackson GA, Ducklow HW, Roman MR (2004) Carbon fluxes through food webs of the eastern equatorial Pacific: an inverse approach. Deep Sea Res I 51:1245–1274

Robinson C, Steinberg DK, Anderson TR, Arístegui J and others (2010) Mesopelagic zone ecology and biogeochemistry—a synthesis. Deep Sea Res II 57:1504–1518

Robison BH, Sherlock RE, Reisenbichler KR, McGill PR (2020) Running the gauntlet: assessing the threats to vertical migrators. Front Mar Sci 7:64

Roman M, Smith S, Wishner K, Zhang X, Gowing M (2000) Mesozooplankton production and grazing in the Arabian Sea. Deep Sea Res II 47:1423–1450

Roman MR, Adolf HA, Landry MR, Madin LP, Steinberg DK, Zhang X (2002a) Estimates of oceanic mesozooplankton production: a comparison using the Bermuda and Hawaii time-series data. Deep Sea Res II 49:175–192

Roman MR, Dam HG, Le Borgne R, Zhang X (2002b) Latitudinal comparison of equatorial Pacific zooplankton. Deep Sea Res II 49:2695–2711

Saint-Béat B, Vézina AF, Asmus R, Asmus H, Niquil N (2013) The mean function provides robustness to linear inverse modelling flow estimation in food webs: a comparison of functions derived from statistics and ecological theories. Ecol Model 258:53–64

Scheinberg RD, Landry MR, Calbet A (2005) Grazing of two common appendicularians on the natural prey assemblage of a tropical coastal ecosystem. Mar Ecol Prog Ser 294:201–212

Selph KE, Landry MR, Taylor AG, Yang EJ and others (2011) Spatially-resolved taxon-specific phytoplankton production and grazing dynamics in relation to iron distributions in the equatorial Pacific between 110 and 140° W. Deep Sea Res II 58:358–377

Sherr BF, Sherr EB, Fallon RD (1987) Use of monodispersed, fluorescently-labeled bacteria to estimate *in situ* protozoan bacterivory. Appl Environ Microbiol 53:958–965

Steinberg DK, Landry MR (2017) Zooplankton and the ocean carbon cycle. Annu Rev Mar Sci 9:413–444

Steinberg DK, Van Mooy BAS, Buesseler KO, Boyd PW, Kobari T, Karl DM (2008) Bacterial vs. zooplankton control of sinking particle flux in the ocean's twilight zone. Limnol Oceanogr 53:1327–1338

Stock C, Dunne J (2010) Controls on the ratio of mesozooplankton to primary production in marine ecosystems. Deep Sea Res I 57:95–112

Straile D (1997) Gross growth efficiencies of protozoan and metazoan zooplankton and their dependence of food concentration, predator–prey weight ratio, and taxonomic group. Limnol Oceanogr 42:1375–1385

Strom SL, Benner R, Ziegler S, Dagg MJ (1997) Planktonic grazers are a potentially important source of dissolved organic carbon. Limnol Oceanogr 42:1364–1374

Stukel MR, Landry MR (2010) Contribution of picophytoplankton to carbon export in the equatorial Pacific: a reassessment of food web flux inferences from inverse models. Limnol Oceanogr 55:2669–2685

Stukel MR, Landry MR, Ohman MD, Goericke R, Samo T, Benitez-Nelson CR (2012) Do inverse ecosystem models accurately reconstruct plankton food web flows? Comparing two solution methods using field data from the California Current. J Mar Syst 91:20–33

Stukel MR, Ohman MD, Benitez-Nelson CR, Landry MR (2013a) Contributions of mesozooplankton to vertical carbon export in a coastal upwelling system. Mar Ecol Prog Ser 491:47–65

Stukel MR, Décima M, Selph KE, Taniguchi DAA, Landry MR (2013b) The role of *Synechococcus* in vertical flux in the Costa Rica upwelling dome. Prog Oceanogr 112-113: 49–59

Stukel MR, Kelly TB, Decima MR (2018) A new approach for incorporating nitrogen isotope measurements into linear inverse ecosystem models with Markov chain Monte Carlo sampling. PLOS ONE 13:e0199123

Taylor AG, Landry MR, Selph KE, Yang EJ (2011) Biomass, size structure and depth distributions of the microbial community in the eastern equatorial Pacific. Deep Sea Res II 58:342–357

Townsend DW, Cammen LM, Holligan PM, Campbell DE, Pettigrew N (1994) Causes and consequences of variability in the timing of spring phytoplankton blooms. Deep Sea Res I 41:747–765

Valencia B, Décima M, Landry MR (2018) Environmental effects on mesozooplankton size structure and export flux at Station ALOHA, North Pacific Subtropical Gyre. Global Biogeochem Cycles 32:289–305

Van den Meersche K, Soetaert K, Van Oevelen D (2009) xsample(): an R function for sampling linear inverse problems. J Stat Software 30:1–15

van Oevelen D, Van den Meersche K, Meysman FJR, Soetaert K, Midderlburg JJ, Vézina AF (2010) Quantifying food web flows using linear inverse models. Ecosystems 13:32–45

Verity PG, Langdon C (1984) Relationship between lorica volume, carbon, nitrogen, and ATP content of tintinnids in Narragansett Bay. J Plankton Res 6:859–868

Verity PG, Stoecker DK, Sieracki ME, Nelson JR (1996) Microzooplankton grazing of primary production at 140° W in the equatorial Pacific. Deep Sea Res II 43: 1227–1255

Vézina AF, Platt T (1988) Food web dynamics in the ocean. I. Best-estimates of flow networks using inverse methods. Mar Ecol Prog Ser 42:269–287

Viviani DA, Karl DA, Church MJ (2015) Variability in photosynthetic production of dissolved and particulate organic carbon in the North Pacific Subtropical Gyre. Front Mar Sci 2:73

Walsh ID, Gardner WD, Richardson MJ, Chung SP, Plattner CA, Asper VL (1997) Particle dynamics as controlled by the flow field of the eastern equatorial Pacific. Deep Sea Res II 44:2025–2047

Ward BA, Dutkiewicz S, Jahn O, Follows MJ (2012) A size-structured food-web model for the global ocean. Limnol Oceanogr 57:1877–1891

Zhang X, Dam HG, White JR, Roman MR (1995) Latitudinal variations in mesozooplankton grazing and metabolism in the central tropical Pacific during the US JGOFS EqPac study. Deep Sea Res II 42:695–715

Editorial responsibility: Shin-ichi Uye, Higashi-Hiroshima, Japan

Submitted: May 13, 2020; Accepted: August 21, 2020
Proofs received from author(s): October 4, 2020